Available online at www.sciencedirect.com
SCIENCE DIRECT
Biochimica et Biophysica Acta 1708 (2005) 209 – 218
BIOCHIMICA ET BIOPHYSICA ACTA
BBA
http://www.elsevier.com/locate/bba

Energetics of primary and secondary electron transfer in Photosystem II membrane particles of spinach revisited on basis of recombination-fluorescence measurements

Markus Grabolle, Holger Dau*

Freie Universität Berlin, FB Physik Arnimallee 14, D-14195 Berlin, Germany

Received 9 December 2004; received in revised form 14 March 2005; accepted 15 March 2005
Available online 2 April 2005

Abstract

Photon absorption by one of the roughly 200 chlorophylls of the plant Photosystem II (PSII) results in formation of an equilibrated excited state (Chl200*) and is followed by chlorophyll oxidation (formation of P680+) coupled to reduction of a specific pheophytin (Phe), then electron transfer from Phe− to a firmly bound quinone (QA), and subsequently reduction of P680+ by a redox-active tyrosine residue denoted as Z. The involved free-energy differences (ΔG) and redox potentials are of prime interest. Oxygen-evolving PSII membrane particles of spinach were studied at 5 °C. By analyzing the delayed and prompt Chl fluorescence, we determined the equilibrium constant and thus free-energy difference between Chl200* and the [Z+,QA−] radical pair to be −0.43±0.025 eV, at 10 μs after the photon absorption event for PSII in its S_3-state. On basis of this value and previously published results, the free-energy difference between P680* and [P680+,QA−] is calculated to be −0.50±0.04 eV; the free-energy loss associated with electron transfer from Phe to QA is found to be 0.34±0.04 eV. The given uncertainty ranges do not represent a standard deviation or likely error, but an estimate of the maximal error. Assuming a QA−/QA redox potential of −0.08 V [Krieger et al., 1995, Biochim. Biophys. Acta 1229, 193], the following redox-potential estimates are obtained: +1.25 V for P680/P680+; +1.21 V for Z/Z+ (at 10 μs); −0.42 V for Phe−/Phe; −0.58 V for P680*/P680+.

Keywords: Chlorophyll fluorescence; Delayed fluorescence; P680; Oxygenic photosynthesis; Redox Potential

1. Introduction

Photosystem II (PSII) is a unique photoenzyme of fundamental importance for atmosphere and biosphere (O_2-formation; crucial role in biomass production by photosynthesis). Crystallographic structure determination has resulted in atomic level models for most parts of the protein–cofactor complex [1–3] and spectroscopic investigations have led to an increasingly complete picture on the structural changes of the Mn_4Ca complex which represents the active site of photosynthetic water oxidation and dioxygen formation [4]. One of the remarkable aspects of the PSII reactions is that, to facilitate water oxidation, the redox chemistry needs to involve unusually positive potentials around +1 V. The efficiency of light-driven water oxidation likely is limited by energetic constraints as has been shown for the entropic contribution to the Gibbs free energy of the oxygen-formation step that stems from dioxygen release [5]. Free-energy differences and redox potentials have been estimated on basis of experimental results ([6–8] and references therein, see also Discussion) and compared to calculated values [9].

Abbreviations: Chl, chlorophyll; DCBQ, 2,6-Dichloro-1,4-benzoquinone; DCMU, 3-(3,4-Dichlorophenyl)-1,1-Dimethylurea; EPPS, 4-(2-Hydroxyethyl)piperazine-1-propanesulfonic acid; ET, electron transfer; F_D, delayed fluorescence signal; F_P, prompt fluorescence signal; F_M, maximum level of prompt fluorescence; F_0, minimum level of prompt fluorescence; ΔG, difference in Gibbs free energy; MES, 2-Morpholinoethanesulfonic acid; MOPS, 3-Morpholinopropanesulfonic acid; P680, primary chlorophyll donor in PSII; Phe, specific pheophytin of PSII; PM, photomultiplier; PSII, Photosystem II; Q_A, primary quinone acceptor of PSII; Q_B, secondary quinone acceptor of PSII; Z or Y_Z or Tyr_Z, Tyr-160/161 of the D1 protein of PSII

* Corresponding author. Tel.: +49 30 838 53581; fax: +49 30 838 56299.
E-mail address: holger.dau@physik.fu-berlin.de (H. Dau).

0005-2728/$ - see front matter © 2005 Elsevier B.V. All rights reserved.
doi:10.1016/j.bbabio.2005.03.007

Significant uncertainties and diverging estimates of ΔG values and redox potentials have prompted us to revisit the PSII energetics.

A direct determination of the redox potentials at the donor side of PSII by redox titration cannot be achieved because exposure of the protein to potentials around +1 V results in numerous destructive side reactions. Furthermore, time-dependent 'working potentials' are likely to be of relevance so that the potentials determined by redox titration may not be sufficient for a discussion of mechanistic questions. In the present work, redox titrations are not employed, but equilibrium constants and thus differences in Gibbs free energy, ΔG, are determined experimentally using the well-known relation:

$$\frac{P_B}{P_A} = K_{AB} = e^{\frac{-\Delta G_{AB}}{kT}}, \quad (1)$$

where P_A and P_B are the equilibrium population of the states A and B, respectively, K_{AB} represents the equilibrium constant, and ΔG_{AB} the corresponding free energy difference.

In Fig. 1, the free energy levels of the relevant PSII states [10] are depicted. Absorption of a photon by one of the roughly 200 chlorophylls of the plant PSII (including the light-harvesting complexes) is followed by rapid excitation energy transfer within the PSII antenna system and population of the different spectral forms of chlorophyll approximately according to a Boltzmann distribution (prevalence of rapid exciton equilibration, REE, as demonstrated elsewhere [11]). The resulting excited antenna state is denoted Chl^*_{200} in Fig. 1. The delocalization and equilibration of the excited state among the PSII chlorophylls leads to a (mostly entropic) free energy difference between Chl^*_{200} and the P680*, the precursor state of the primary charge separation ([11] and references therein). In the likely case of a multimeric P680*-state only the enthalpic contribution to the free energy of P680* is considered which is estimated to be around 1830 meV above the ground state level (energy of a 680 nm photon). Formation of P680* may initiate the primary charge separation leading to reduction of a specific pheophytin (Phe) and formation of $P680^+$, the oxidized primary donor. The thus formed radical pair, $P680^+Phe^-$, is the precursor for the secondary charge separation leading to reduction of the quinone denoted as Q_A and thus the formation of the $P680^+Q_A^-$ radical pair. Subsequently, $P680^+$ becomes reduced by electron donation from a redox-active tyrosine, the Tyr-161 of the D1-protein of PSII (denoted as Tyr_Z, Y_Z or simply Z; Tyr-161 for plant, but Tyr-160 for cyanobacterial numbering). This electron transfer (ET) is multiphasic with the fast components in the sub-microsecond range and slower microsecond components suggesting that the ns-ET is followed by a multiphasic energetic relaxation corresponding to a time-dependent ΔG_3 ([12–14]; for review, see [15]).

In the following, it is assumed that, after completion of the respective ET reaction, the reversibility of the process

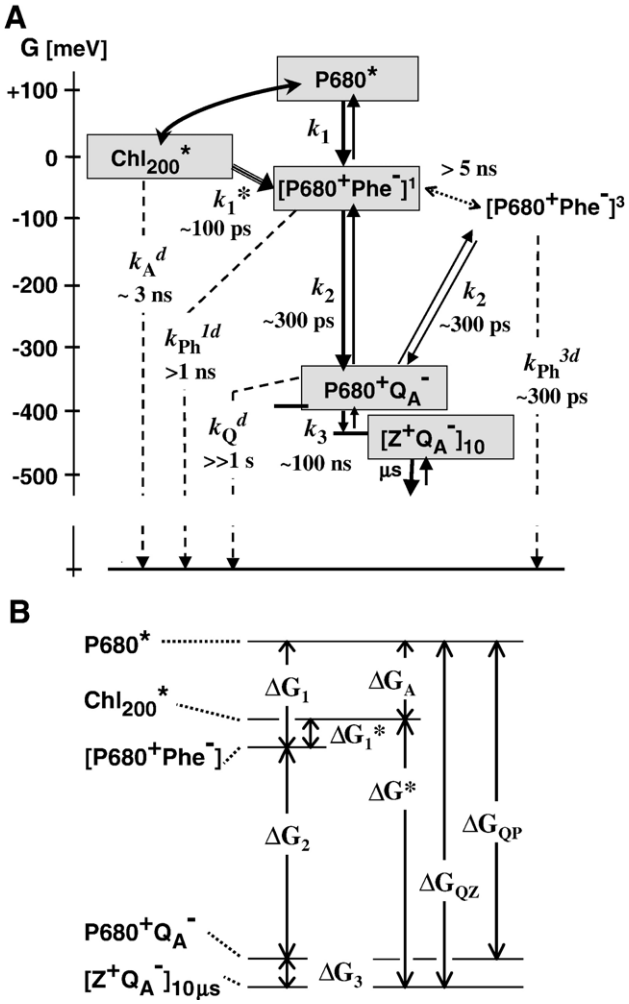

Fig. 1. Energy level diagram for the PSII-states of interest. Abbreviations used to denote differences in Gibbs free energy are indicated in B; the ΔG values itself are derived and discussed further below. In A, k_1^* is the rate constant for excited antenna state decay by primary charge separation in the plant PSII, which depends on the PSII antenna system and is distinctly different from k_1, the clearly greater intrinsic rate constant of primary charge separation [11]. The meaning of the other rate constants is as follows: k_2, electron transfer (ET) from Phe to Q_A; k_3, ET from Z to $P680^+$; k_A^d, excited state decay by fluorescence and thermal dissipation; k_{Ph}^{1d} and k_{Ph}^{3d}, decay of the singlet state $[P680^+, Phe^-]^1$ and the triplet state $[P680^+, Phe^-]^3$, respectively, by other ways than Q_A reduction or the recombination that is coupled to repopulation of Chl^*_{200}, the excited antenna state; k_Q^d, decay of the $P680^+Q_A^-$ radical pair by other ways than forward ET from the Z to $P680^+$ or backward ET from Q_A^- to Phe. In A, for selected rate constants the approximate values of the corresponding time constants, i.e., the reciprocal rate constants, are given. The G value of the Chl^*_{200} state is chosen to be zero. The energy of P680* is about 1830 meV above the ground state level (absence of any excited state or radical pair); decay processes leading directly or indirectly to repopulation of the ground state are marked by dashed lines. For the given rate constant values see, e.g., k_1^* and k_2 [11]; k_A^d, [27]; k_{Ph}^{3d}, [16]; and k_Q^d, [7]. There is no data on the value of k_{Ph}^{1d}, but a reasonable photochemical quantum yield requires a value clearly smaller than 1 ns^{-1}.

results, to a first approximation, in an equilibrium population according to Eq. (1) for the following states in Fig. 1: Chl^*_{200}, $[P680^+Phe^-]^1$, $[P680^+Q_A^-]$, and $[Z^+Q_A^-]$. This assumption is

valid only if the loss processes do not affect the populations significantly requiring that $k_1^* \gg k_A^d$, $k_2 \gg k_{Ph}^{1d}$ and $k_3 \gg k_Q^d$. The value of k_{Ph}^{1d} is unknown, but the common assumption that the quantum yield of the PSII charge separation reactions is close to unity implies that *all* loss processes are slow in comparison to the respective forward reaction.

In Fig. 1 also the triplet state of the primary radical pair is considered. The primary charge separation itself results in formation of the singlet state of the primary radical pair and the intersystem crossing is slow (>5 ns) in comparison to secondary ET [16]. The recombination decay of $P680^+Q_A^-$ is believed to proceed mostly via the triplet state of the primary radical pair [6,7]. The estimated rate for the $[P680^+Phe^-]^3$-decay, which involves also the formation of Chl triplet states, is comparatively high so that population of this state may well be below the predicted equilibrium value. Due to the slow intersystem crossing, however, the comparatively fast triplet decay will not affect the population of $[P680^+Phe^-]^1$ so that the rationale used in the following is not compromised by the non-equilibrium population of $[P680^+Phe^-]^3$.

In the present work, the equilibrium populations of the excited antenna state, Chl_{200}^*, and the $Z^+Q_A^-$ state reached at 10 μs after the photon absorption event are used to determine the respective free energy difference, ΔG^*, according to Eq. (1). At 10 μs, the $Z^+Q_A^-$ state is populated in about 80% of all PSII [13]. The corresponding Chl_{200}^* population becomes experimentally accessible by measurements of the chlorophyll fluorescence emitted at 10 μs after the photon absorption event because this fluorescence level is determined by the $Chl_{200}^* - Z^+Q_A^-$ equilibrium constant which equals $e^{-\Delta G^*/kT}$.

The used rationale relies on the assumption that the charge recombination reactions repopulate the same excited state of the PSII antenna system as it is populated within a few picoseconds after the absorption of a photon by rapid exciton equilibration [11]. This is verified by a comparison of the high-precision emission spectra of delayed and prompt chlorophyll fluorescence. Then, the value of ΔG^* is determined and its pH-dependence is assessed. Based on the ΔG^* value and previously published results the various free energy differences in Fig. 1 are derived and the putative implications for the redox potentials of PSII cofactors are discussed.

2. Materials and methods

2.1. PSII membrane particles and buffer media

Highly active PSII membrane particles were prepared from spinach as described in [17] and stored at −80 °C at a Chl concentration of 1.5–2.5 mg Chl/mL in a buffer containing 1 M glycine betaine, 15 mM NaCl, 5 mM $MgCl_2$, 5 mM $CaCl_2$, and 25 mM MES, pH 6.2 (buffer A). Before and after freezing, the oxygen-evolution activity assessed at 28 °C in the presence of 1 M glycinebetaine had been 1200–1400 μmol O_2 per mg Chl and hour. Before use, the samples were thawed for at least 1 h on ice and washed by dilution in buffer A and centrifugation. The resulting pellet was resuspended in buffer A to a Chl concentration of 10 μg/mL and stored on ice until use. For measurement of the pH-dependence, the pellet was resuspended in a buffer containing 1 M glycine betaine, 25 mM MES, 25 mM MOPS, 25 mM EPPS, 10 mM NaCl, 5 mM $MgCl_2$ and 5 mM $CaCl_2$; the pH was adjusted by addition of HCl and NaOH. One minute before the measurement, the electron acceptor DCBQ was added to yield a concentration of 20 μM. The addition of DCBQ caused a slight fluorescence quenching (20% at the F_0 level; 40% at the F_M level). In the absence of DCBQ the period-four oscillations are found to end abruptly after ~10 flashes, but otherwise essentially identical values are obtained for the kinetic and energetic parameters discussed in the present work.

2.2. Spectra of prompt and delayed fluorescence

Prompt and delayed fluorescence spectra were collected using a commercial fluorometer (Cary Eclipse, Varian; red-enhanced detection photomultiplier, excitation by Xenon flashes at 435±1 nm, detection at the indicated center wavelength ±1 nm at a band width of 2.5 nm, sample temperature of 288±1 K). To obtain the spectra of the delayed fluorescence, emission was integrated from 200 μs to 2 ms after the excitation flash. All spectra were corrected for the wavelength-dependent sensitivity of monochromator and photomultiplier. For further details, see [18].

2.3. Kinetic fluorescence measurements

In the delayed fluorescence experiment, the dark adapted samples were excited by a saturating Laser flash of 2 mJ/cm^2 (Continuum Minilite II, $\lambda = 532$ nm, fwhm of 5 ns, time between flashes of 0.7 s). The Laser beam was widened by lenses and shaped by an aperture to yield approximately homogenous illumination of a quadratic area of 1 cm^2 matching the width of the used optical cuvette. Pulse intensities were determined using a Nova-Laser-Power/Energy-Monitor, measuring head PE10 (Ophir Optronics).

To avoid saturation of the detector system caused by the strong prompt fluorescence of the probe during laser excitation, a gated photomultiplier was used (Hamamatsu R2066; PMT Gated Socket Assembly C1392-55; anode voltage, 1000 V; anode resistor, 2.2 kΩ; gating voltage, 240 V applied from 7 μs before to 3 μs after the Laser flash). Scattered Laser light was blocked by a combination of two long-pass filters (LINOS Photonics, DT-red and DT-magenta with cut-off wavelength 600 and 632 nm, respectively). After amplification (Tektronix AM502, band width of 300 kHz), the signal was sampled at 1 MHz by a 12-bit PC-card (ADLINK, PCI 9812).

The data were corrected for an artefact of the detector system predominantly due to excitation of delayed fluorescence in the glass or cathode material of the photomultiplier by the strong prompt fluorescence of the PSII particles as well as by scattered light of the excitation flash. The correction procedure is described in the following. If the sample is excited by laser flashes with an intensity above the saturation level, all PSII centers are hit and the delayed fluorescence is maximal. Ideally, a further increase in the flash energy should not result in any significant intensity increase of the delayed fluorescence. Such an increase, however, is observed. The amplitude of this non-saturating contribution to the fluorescence signal is found to increase linearly with the laser-pulse intensity. To correct for the artefact contribution, delayed fluorescence measurements were carried out at flash intensities of 2 and 4 mJ/cm^2. The difference of the two measurements performed on PSII membrane particles at flash intensities of 2 and 4 mJ/cm^2 (all other experimental conditions remain unchanged) yields the artefact contribution caused by the flash of 2 mJ/cm^2. This calculated difference signal can now be subtracted from the signal measured at 2 mJ/cm^2. The contribution of the artefact to the total signal at 10 μs after the exciting flash typically was below 20% for the 3rd flash signal (and smaller at later times).

DCMU induction curves were measured with the same detection system as the delayed fluorescence. For excitation of the sample, a continuous wave Laser pointer (Atelier Rieter, Germany) with an emission wavelength of 532 nm was used and shaped by lenses and apertures to yield the same irradiated area as in the case of the excitation by ns Laser pulses. The offset in the prompt fluorescence signal caused by scattered light had been negligibly small. The light intensity at the cuvette was determined to be 16 μmol photons per m^2 and s (measured by Light Meter LI-189, LI-COR).

For determination of the absorption cross-section of PSII at 532 nm, the Laser flash-energy dependence of the prompt chlorophyll fluorescence was measured with a commercial fluorometer (FL 3000, Photo Systems Instruments, Czech Republic) using light pulse of 8 μs duration to determine the intensity of the prompt fluorescence at selected times after the ns-Laser pulse; the maximum level of the prompt chlorophyll fluorescence obtained at about 140 μs after the flash was used for determination of the absorption cross-section.

The temperature of the sample was controlled using a combination of water bath and circulator (Haake, DC50) and a laboratory built water-jacketed cuvette holder.

3. Results

3.1. Delayed fluorescence—spectra and decay curves

The emission spectra of the promptly emitted chlorophyll fluorescence and delayed fluorescence emission are essentially identical (Fig. 2) demonstrating that, as predicted by the rationale outlined above, prompt and delayed fluorescence are determined by the same equilibrium distribution of excited states in the antenna system of PSII [11,19].

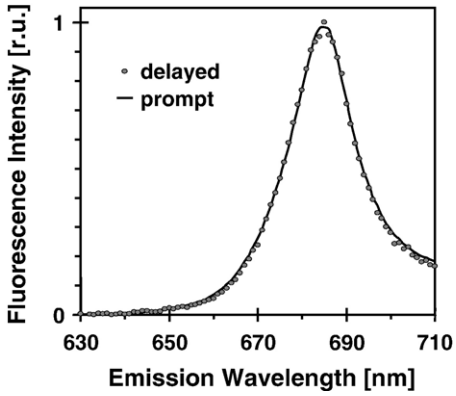

Fig. 2. Comparison of emission spectra of prompt and delayed chlorophyll fluorescence. Both spectra were measured for excitation at 435 nm by μs-pulses delivered by a Xenon-flash lamp. To obtain the delayed fluorescence spectrum, the fluorescence intensity was integrated from 200 μs to 2 ms.

The time courses of the intensity of the delayed fluorescence, $F_D(t)$, depend on the flash number; a damped oscillation with a period of four is clearly visible in Fig. 3. The periodicity results from the advancement of PSII in its S-state cycle and indicates that contribution stemming from inactive PSII centers are, in the context of the present work, negligible. The delayed fluorescence at 2 ms is mostly determined by the PSII undergoing the oxygen-evolving $S_3 \rightarrow S_0$ transition on the respective flash; the resulting O_2-evolution pattern is characterized by a relatively small miss parameter of less than 10%. The oscillatory pattern itself will be subject of future investigations (Grabolle and Dau, work in progress). In the following, we will focus on the value reached at 10 μs after the third saturating Laser flash.

3.2. Rationale for determination of ΔG^*

As shown in the introduction section, for an ensemble of PSII the excited antenna state is populated according to the free energy difference, ΔG^*, between the excited-antenna state and the radical-pair state reached at a given time. At 10 μs, this is the $Z^+Q_A^-$ state so that the delayed fluorescence signal in Volt is given by (note that the actual ΔG values are negative):

$$F_D = S\ c_P\ e^{\Delta G^*/kT} \tag{2}$$

with

$$c_P = n_{Z^+Q_A^-}/n_{PSII} \tag{3}$$

and

$$S = C_M k_F n_{PSII}, \tag{4}$$

where C_M represents the efficiency of the fluorescence detection system (in units of Volts per emitted photon·s^{-1} per PSII, which equals V × s), k_F is the rate constant for

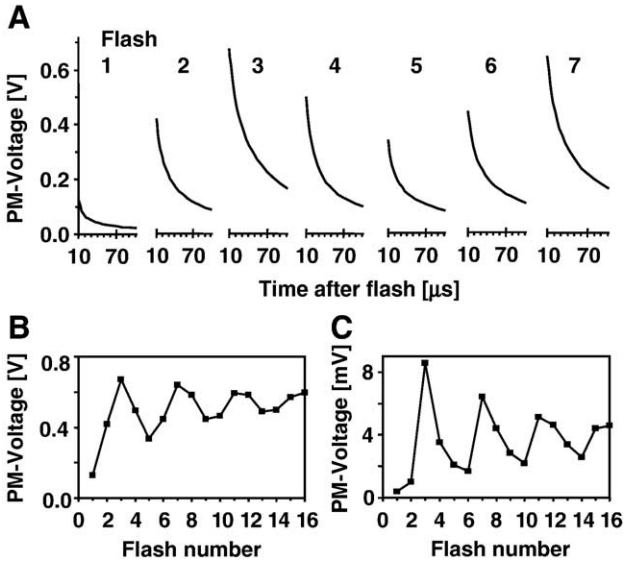

Fig. 3. Flash pattern of delayed fluorescence. A train of saturating ns-Laser flashes was applied to dark-adapted PSII membrane particles (at 5 °C). In A, for each of the first 7 flashes, $F_D(t)$ is shown for a time period of 10 to 100 µs after the flash. In B and C, the intensity of the delayed fluorescence is shown at 10 µs and at about 2 ms after the flash, respectively. The value for the intensity at 2 ms was obtained by averaging the measured intensities in the time range from 1 to 3 ms. (The lines in B and C simply connect the data points and have not been obtained by simulations).

fluorescence emission of the PSII antenna system (around $5{\cdot}10^7$ s^{-1}), and n_{PSII} is the number of PSII in the sample volume. The c_P value gives the fraction of PSII in the $Z^+Q_A^-$ state which is, due to population of the $P680^+Q_A^-$ state, smaller than unity (around 80% at 10 µs after the third flash).

A few explanatory remarks on Eqs. (2)–(4) may be useful. The reciprocal value of c_P corresponds to the value of a partition function which takes into account all radical pairs and excited states. Assuming an equilibrium distribution, the product of the exponential factor and c_P gives directly the fraction of PSII in the excited-antenna state, which is at, e.g., 10 µs already extremely small (on the order of 10^{-7}). The detected signal (F_D in Volt) equals this fraction times the probability for fluorescence emission per time interval of a PSII in its excited antenna state (k_F) times the total number of PSII (n_{PSII}) times the efficiency of the detection system (C_M). By the detection system a rate of emitted photons (photons per time interval) is converted into a voltage leading to a unit of C_M of Volts times second.

Eq. (2) provides a direct relation between the level of delayed fluorescence and the ΔG^* provided the value of the sensitivity factor, S, is known. The value of S was determined by a calibration experiment involving measurement of the promptly emitted chlorophyll fluorescence.

3.3. Determination of S, the sensitivity factor

In Fig. 4A, a so-called DCMU induction curve of the prompt PSII fluorescence is shown (see [20] for review). The Q_A-Q_B electron transfer is blocked in the presence of the DCMU. Upon onset of an actinic light, the fraction of PSII with Q_A in its reduced state continuously increases leading to an increase in the prompt Chl fluorescence from the F_0 level (Q_A oxidized in all PSII) to the F_M level (Q_A reduced in all PSII). This prompt fluorescence experiment and the delayed fluorescence measurements of Fig. 3 were carried out on the same day using the same detection

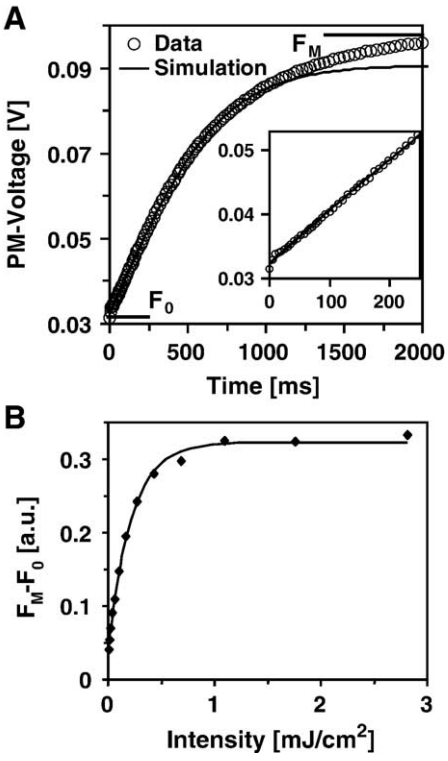

Fig. 4. Fluorescence induction curve of DCMU-inhibited PSII membrane particles (in A) and Laser-flash-intensity dependence of the increase in the prompt fluorescence induced by a single-turnover Laser flash (in B). In A, at $t=0$ a rapid shutter opened (within less than 1 ms) facilitating illumination of the dark-adapted PSII membrane particles suspended in a buffer containing DCMU (40 µM DCMU added to the buffer used in the experiment of Fig. 3) with light of a cw-Laserdiode (532 nm, intensity of 16 µE). The induction curves of the prompt fluorescence were measured using the same experimental set-up used for detection of the delayed fluorescence traces of Fig. 3; the y-scales (PM-Voltage) are directly comparable. The solid line represents a simulation of the DCMU induction curves using the following parameters: $R_A=2.15$ s^{-1}, $p=0.32$ (connectivity parameter describing inter-PSII excitation-energy transfer), $\phi_A=2.23\times10^{-19}$ m^2, $I_A=16$ µE. These parameters were determined by a least-square fit where the error sum had been calculated only for $t\leq1$ s. The slowly rising exponential component frequently explained by a minority fraction of $PSII_\beta$-units is not considered in the simulation so that a clear deviation is observed for $t>1$ s. In B, the flash-energy dependence of the increase in the prompt fluorescence caused by a single-turnover Laser-flash (~5 ns half-width, 532 nm) and probed by a weak LED pulse at 140 µs after the Laser flash is shown. The prompt fluorescence level measured prior to the Laser-flash (F_0 level) was subtracted. The solid line was obtained by a simulation with an absorption cross-section of 1.75×10^{-19} m^2 per PSII at 532 nm (without taking into account PSII connectivity and PSII heterogeneity).

system, identical sample volume and concentration of PSII membrane particles.

The measured intensity of the prompt fluorescence in the induction curve experiment of Fig. 4 is given by

$$F_p = C_M \phi_A I_A k_F \tau_F n_{PSII}. \quad (5)$$

so that the sensitivity factor of Eq. (4) is obtained by:

$$S = C_M k_F n_{PSII} = \frac{F_p}{\phi_A I_A \tau_F} \quad (6)$$

where ϕ_A is the absorption cross-section per PSII at the wavelength of the actinic light (in m^2), I_A is the intensity of the actinic light (in photons per m^2 and s), and τ_F is the mean excited state lifetime. We note that Eq. (6) is valid at any time in the induction experiment because F_P and τ_F are time dependent, but their ratio is constant. The value of τ_F that corresponds to the F_P value at the initial F_0 level has been determined for PSII membrane particles to be 240 ps [11].

Also determination of the effective rate of photon absorption,

$$R_A = \phi_A I_A, \quad (7)$$

is facilitated by the fluorescence induction experiment. Assuming a quantum yield of Q_A reduction close to unity, the rate of the fluorescence increase in the induction experiment of Fig. 4 is mostly determined by R_A, which is the product of light intensity, I_A, and the absorption cross-section per PSII at the wavelength of the actinic light, ϕ_A (for further details see [21] and references therein). Simulation of the DCMU curve of Fig. 4A lead to a value of 2.15 s^{-1} for R_A. This R_A value corresponds to ϕ_A, the PSII absorption cross-section at 532 nm, of $2.23 \cdot 10^{-19}$ m^2 (for I_A=16 μmol photons m^{-2} s^{-1}). Neglecting the influence of PSII connectivity, a mono-exponential simulation of the DCMU induction curves of Fig. 4 leads to a ϕ_A value of $1.56 \cdot 10^{-19}$ m^2. As shown in Fig. 4B, essentially the same value is obtained using an independent approach, namely the determination of ϕ_A by analysis of the flash-energy dependence of the increase in prompt chlorophyll fluorescence induced by the flash [22], confirming the used rationale for interpretation of the DCMU induction curves.

Thus, knowing the values of F_D, F_P, R_A, and τ_F, the value of ΔG^* can be calculated according to:

$$\Delta G^* = kT ln\left(F_D c_P^{-1} S^{-1}\right) \quad (8)$$

where the sensitivity factor, S, is obtained by means of Eqs. (6) and (7).

3.4. Determination of ΔG^* and uncertainty range

We have chosen to determine ΔG^* for the state reached at 10 μs after the third saturating Laser flash meaning that the respective intensity of the delayed fluorescence is of relevance leading to a F_D voltage of 0.663 V (Fig. 3) with an estimated maximal inaccuracy of ±10% (due to noise and inaccuracy in the Chl concentration). The presence of about 20% of PSII in the $P680^+Q_A^-$ state [13] leads to a c_P value of 0.8±0.08.

A value of R_A of 2.15 s^{-1} is obtained by analysis of the DCMU induction curves. Mostly due to the neglect of putative heterogeneities in the PSII antenna size ([20,23], minority fractions of $PSII_\beta$ units are neglected) and conceivable imprecision in modeling the inter-PSII excitation energy transfer (neglect of dimeric PSII organization), the inaccuracy range may be as large as ±25%. For determination of F_P and τ_F, we choose the F_0 level where, according to Fig. 4, the F_P value is 0.032 V (±10%). In [19] the excited state lifetime at the F_0 level was determined to be 240 ps for a similar preparation of PSII membrane particles; its estimated uncertainty of ±10% takes into account the minor differences between the experimental conditions used in [19] and the ones of the present work. Eventually, we obtain a ΔG^* value of −434 meV and an estimated uncertainty range of ±17 meV. As shown in Fig. 5, ΔG^* is essentially pH independent.

Noteworthy, a temperature-dependent quenching of the F_M and F_0 level of the prompt Chl fluorescence is observed (decrease in F_0 and F_M by 25% and 45%, respectively, for an increase in temperature from 0 °C to 30 °C, data not shown). This observation suggests that at higher temperatures a decrease in the Chl^*_{200} population is caused by an increased thermal deactivation of excited antenna states rendering the assumption of negligible loss processes less stringent for elevated temperatures. Therefore, the fluorescence measurements were carried out at 5 °C, a temperature at which also the miss probability was found to be minimal (<10%). (We have verified by extensive analysis of emission and excitation spectra that the coupling between

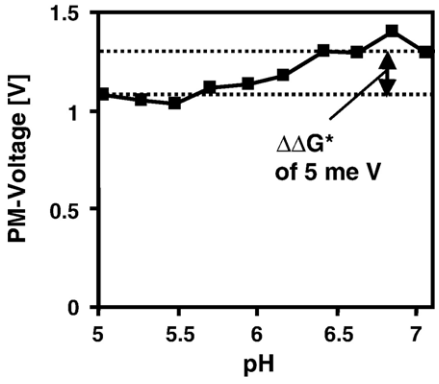

Fig. 5. pH-dependence of the delayed fluorescence intensity. The F_D value was measured at 10 μs after the third Laser flash (at 20 °C). Calculation of the corresponding ΔG^* value by Eq. (8) indicates that the range between the two dotted lines corresponds to a $\Delta\Delta G^*$ of 5 meV. The shown F_D values are not corrected for the fraction of PSII that is not in the S_3 state prior to the third Laser flash. Since this fraction increases with decreasing pH, the corresponding correction reduces further the minor pH-dependence visible in the figure (not shown). It should be noted that the data shown in Fig. 3 had been collected at 5 °C, whereas the pH-dependence was studied at 20 °C leading to clearly higher F_D voltages at 10 μs (20 °C) than in Fig. 3 (5 °C).

peripheral light-harvesting complexes and the PSII core complexes is not affected by the temperature; rapid exciton equilibration including the complete PSII complex prevails over the full range from 0° to 30 °C [18].)

3.5. Minor corrections

In the following corrections are discussed which affect the ΔG^* value only slightly (by 5 meV), but result in an increase in the uncertainty range by 8 meV. The used F_D value had been determined at 10 μs after the third flash and it was assumed that, to a first approximation, 100% of the PSII had been in the S_3 state. In separate experiments, we obtained an estimate of the miss-probability (*m* equals about 9%) and of the fraction of PSII with blocked Q_A-Q_B electron transfer (about 18%), which are also denoted as non-Q_B units (data not shown, see also [20]). (1) Due to the latter PSII fraction, the F_D value is reduced by 18±5% which corresponds to a ΔG^* correction by +4±1 meV. (2) The miss events (9±3%) lead to a reduction of F_D approximately by 8±3% which corresponds to a $\Delta\Delta G^*$ of +2±1 meV. (3) We furthermore roughly estimate that the F_D reduction due to thermal losses ranges from 10% to maximally 50% ($\Delta\Delta G^*$ of +6±4 meV). (4) Whenever in an individual PSII, a recombination event takes place and leads to repopulation of the excited antenna state, the Q_A of this individual unit is in its oxidized state, whereas the P680 is reduced so that, on a first glance, the Q_A^- or $P680^+$ concentration in the sample will not affect the F_D value. However, due to excitation energy transfer between PSII units the average redox state of the PSII in the sample can affect the F_D value. In the PSII where the excited state is created by charge recombination another charge separation can take place thereby leading to a low excited state lifetime (F_0 state). After excitation energy transfer to a neighboring PSII in the high-fluorescent state (F_M) with reduced Q_A and without oxidized P680 (~80% of all PSII at 10 μs after the third laser flash), the probability for fluorescence emission is increased. On basis of the connectivity parameter, *p*, determined by simulation of the DCMU induction curve (Fig. 4), we roughly estimate that the increase in F_D resulting from PSII connectivity amounts to 25–45%. This figure corresponds to a negative $\Delta\Delta G^*$ of −7±2 meV. Summation of the four individual corrections results in a total correction by +5 meV and an increase in the uncertainty range by 8 meV. Consequently, we arrive at the corrected ΔG^* value of −429 ± 25 meV given in Table 1. The implications of the thus determined ΔG^* value for crucial energetic parameters of PSII are summarized in Table 1 and discussed in the following.

3.6. Calculation of further ΔG values and redox potentials

The determined ΔG^* value refers to the free energy of an excited antenna state characterized by equilibration of the excited state over ~200 chlorophylls of the PSII antenna system (see also Fig. 2) and thus resulting in a significant entropic contribution to the free energy of the Chl^*_{200} state [19,21,24,25]. The free energy of the P680* state (or its enthalpic contribution in the case of a multimere of Chl representing P680) is estimated to be by about 110 meV higher than the free energy the Chl^*_{200} state [11] leading to a free-energy difference between the P680* state and the $[Y_Z^+,Q_A^-]_{10\ \mu s}$-state of −540 meV (row no. 2 in Table 1). By inspection of Fig. 1 in [13], at 10 μs after the third flash, we determined an equilibrium constant for the Tyr_Z oxidation by $P680^+$ that corresponds to a ΔG value of 38 meV, a figure that leads to ΔG_3 (row no. 3 in Table 1). In [11], analysis of ps-fluorescence decays of PSII membrane particles on basis of the reversible-radical-pair model [24] were extended by explicit consideration of the exciton equilibration component and a ΔG_1 value of −161 meV has been obtained, a number which is in good agreement with results reported in [26,27]. Using the value of −161 meV, ΔG_2 is obtained (row no. 4 in Table 1).

To relate the experimentally determined ΔG values to redox potentials, we assume that the redox potential differences, $\Delta E_{1/2}$, correspond to free energy differences

Table 1
Derived energy differences and redox potentials

	Additional assumptions	Quantity	Value
1	results of this work; τ_{F0}=240 ± 50 ps[a]	ΔG^* of $Chl_{200}^* \leftrightarrow [Y_Z^+,Q_A^-]_{10\ \mu s}$	−429 ± 25 meV
2	antenna entropy contribution, ΔG_A, of 111 ± 6.5 meV[a]	ΔG_{QZ} of $P680^* \leftrightarrow [Y_Z^+,Q_A^-]_{10\ \mu s}$	−540 ± 32 meV
3	ΔG_3 of $[Y_Z,P680^+] \leftrightarrow [Y_Z^+,P680]$ at 10 μs equals 38 ± 10 meV[b]	ΔG_{QP} of $P680^* \leftrightarrow [P680^+,Q_A^-]$	−502 ± 42 meV
4	ΔG_1 of $P680^* \leftrightarrow [P680^+,Phe^-]_{1ns}$ equals 161 meV or ΔG_1*=50 ± 7 meV[a]	ΔG_2 of $[P680^+,Phe^-] \leftrightarrow [P680^+,Q_A^-]$	−341 ± 42 meV[d]
5	$E_{P680*} - \lvert\Delta G_{QP}\rvert$ equals redox potential difference, $\Delta E_{1/2}^{QP}$=	$E_{1/2}(P680/P680^+) - E_{1/2}(Q_A^-/Q_A)$	1.33 V
6	$E_{1/2}(Q_A^-/Q_A)$=−80 mV[c] $E_{1/2}(Q_A^-/Q_A) + \Delta E_{1/2}^{QP}$=	$E_{1/2}(P680/P680^+)$	1.25 V
7	$E_{1/2}(P680/P680^+) - \lvert\Delta G_3\rvert$=	$E_{1/2}(Y_Z/Y_Z^+)_{10\ \mu s}$	1.21 V
8	$E_{1/2}(Q_A^-/Q_A) - \lvert\Delta G_2\rvert$=	$E_{1/2}(Phe^-/Phe)_{1ns}$	−0.42 V
9	$E_{1/2}(Q_A^-/Q_A) - \lvert\Delta G_{QP}\rvert$=	$E_{1/2}(P680^*/P680^+)_{1ns}$	−0.58 V

All numbers were determined for PSII membrane particles prepared by similar protocols (all based on the use of the detergent Triton X-100). The given ranges represent an attempt to estimate the maximal error including the error in the measurements itself as well as systematic errors.

[a] [11].
[b] [13].
[c] [28].
[d] The uncertainty in the antenna entropy does not contribute because the value of ΔG_1^* is directly calculated from the data of [11].

according to: $e\Delta E_{1/2}=\Delta G$ (used in row no. 5–9 in Table 1; e represents the elementary charge). To obtain absolute redox potentials, the potential of the Q_A^-/Q_A couple as determined by redox titrations in [28] is used, directly leading to the estimates of the redox potentials of the primary donor (P680/P680$^+$), the Tyr_Z (Y_Z/Y_Z^+) and the primary acceptor (Phe^-/Phe) given in Table 1 in row nos. 6 to 8.

4. Discussion

4.1. Determined ΔG values

The free energy difference, ΔG^*, between the excited antenna state and the $Z^+Q_A^-$ state acquired at 10 μs after the photon absorption event that initiates the $S_3 \rightarrow S_0$ transition is found to be -429 ± 25 meV (at 5 °C). This free energy difference is calculated on basis of the corresponding equilibrium constant which was experimentally directly determined for highly active PSII membrane particles. The error range of ±25 meV appears to be small, but corresponds to a sizable range in the equilibrium constant of $1{\cdot}10^7$ to $8{\cdot}10^7$. The given uncertainty range represents a maximum error meaning an estimated worst-case value with respect to the considered uncertainties. We note that at 10 μs after the initiating Laser flash, an energetic relaxation of the $Z^+Q_A^-$ radical-pair is in progress [12–15]. Thus, ΔG^* does not necessarily represent a true free energy difference. This uncertainty in the meaning of ΔG^*, however, does not affect ΔG_{QP} and therefore not the ΔG values and redox-potential estimates given in rows 3–6, 8, and 9 in Table 1.

Analysis of the activation energy for charge recombination in Mn-depleted PSII has provided indications for a ΔH_2 as low as around −160 meV ([6,29] suggesting a negative entropic contribution around 180 meV ($-T\Delta S_2 \approx -180$ meV). In D1/D2 reaction center particles, below 200 K, the ΔG_1 appears to be purely entropic [30]. Investigating Mn-depleted PSII core complexes of cyanobacteria, Hou et al. [31] determined the enthalpy change for the reactions leading to the $Z^+Q_A^-$ state reached at ~1 μs (at pH 6) to be −0.9 eV, an astounding value that requires a sizable positive entropic contribution ($-T\Delta S_{QZ} \gg +100$ meV) to obtain reasonable ΔG_{QZ} values (for a review on the energetics of photosynthetic systems investigated by photoacoustic techniques, see [32]). The Mn-depleted PSII or D1/D2 reaction center particles may differ significantly – with respect to structure, kinetics and energetics – from the oxygen-evolving PSII particles used in the present investigation. Overall, we feel that – due to the involved experimental (and conceptual) difficulties and inconsistencies – the existence, magnitude and origin of putative entropic contributions remains an open question that requires further investigations.

The free energy difference ΔG^* is found to be largely pH independent (Fig. 5) suggesting that none of the reactions leading within 10 μs to the $Z^+Q_A^-$ radical pair is coupled to proton uptake or release. The here observed pH independence is in agreement with the pH-independent redox potential of Q_A [28].

The analysis of ps-fluorescence decay measurements on basis of the reversible-radical pair model [24] has been repeatedly carried out for PSII membrane particles [11,26,27] consistently leading to values close to −45 meV and −160 meV for ΔG_1^* and ΔG_1, respectively. The validity of the underlying assumption of rapid exciton equilibration has been confirmed in [11] and is further supported by data of Fig. 2. Since in [11] the equilibration process itself is considered in the determination of molecular rate constants, the in [11] obtained ΔG_1 and ΔG_1^* values may be the most precise and therefore are used in Table 1. (In Table 1 of [11], the ΔG_1^* value itself is not explicitly stated. It can be calculated from the corresponding equilibrium constant which equals k_1^*/k_{-1} with $k_1^*=k_1^{int} n_{Chla}^{-1} c_E$, where n_{Chla} is 140 and the energy concentration factor, c_E, equals 1.35.) Since the rationale is well established, we feel that the thus obtained values for ΔG_1 and ΔG_1^* are sufficiently precise to allow for meaningful estimates of ΔG_{QP} and ΔG_2.

The ΔG_1 and ΔG_1^* value and the relatively uncritical estimate of ΔG_3 leads to values for ΔG_2, the free energy difference of the Phe→Q_A electron transfer, of −341 meV. Van Gorkom et al. found by analysis of the fluorescence emission induced by an electrical pulse in osmotically swollen thylakoid membranes (electroluminescence) that $|\Delta G_2|$ is greater or equal than 330 meV [33]; and by evaluation of the kinetics of the Q_A^- P680$^+$ recombination in Mn-depleted PSII they determined a maximal value of 360 meV [8]. Based on analysis of the Q_A^- decay (in the time range of seconds) by recombination of the $S_2Q_A^-$ state towards the S_1Q_A state in DCMU-inhibited cells of wildtype and mutants of the cyanobacterium *Synechocystis*, Rappaport et al. [7] concluded that the value of ΔG_2 is close to −360 meV. We note that Van Gorkom et al. and Rappaport et al. obtained an estimate of ΔG_2 by means of approaches which differ distinctly from the one used in the present investigation. Reassuringly, a ΔG_2 value close to −345 meV consistently is obtained, irrespective of the used approach and the chosen organism.

4.2. PSII redox potentials

The PSII is characterized by an unusually positive potential of the redox components at its donor side. This commonly accepted assertion mostly is based on the requirement of potentials around +1 V for the oxidation of water; experimental results on the redox potential, however, are scarce. Direct determination of such positive potentials by redox titrations are, on principle, impossible so that more or less indirect estimates need to be employed. The here estimated values (Table 1, Fig. 6) rely on three assumptions: (i) the experimentally determined ΔG values (Table 1) are

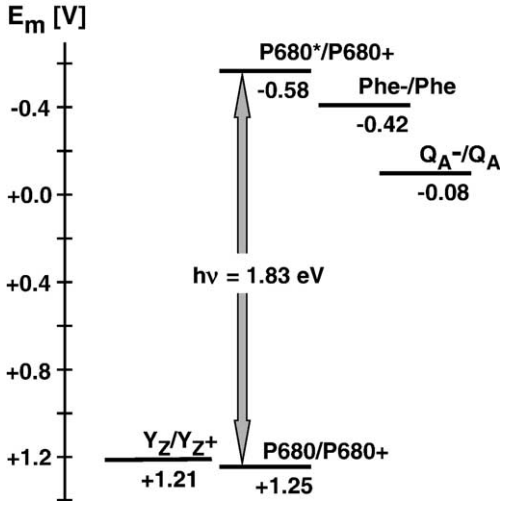

Fig. 6. Estimated redox potentials of PSII cofactors involved in primary and secondary electron transfer (for details, see text body).

sufficiently precise; (ii) $\Delta G/e$ equals the redox-potential difference; and (iii) the Q_A^-/Q_A potential determined by Krieger et al. [28] represents a sufficiently reliable 'anchor point' of the redox potential scale.

Determination and uncertainty in the ΔG values is discussed above and, in our opinion, does not represent the most important source for possible errors in the redox-potential estimates of Table 1. For the Q_A^-/Q_A potential, a wide range of values had been reported in the past (−0.35 to +0.15 V; see [28]). Krieger et al. [28] thoroughly reinvestigated the Q_A^-/Q_A potential by redox titration of suspensions of PSII membrane particles and eventually obtained a value of −81±16 mV (standard deviation of ±16 mV; for fully intact PSII, without using any redox mediators or Q_B site inhibitors or cryo-protocols), a value we consider to be reasonably reliable.

The functionally relevant 'working potential' of Q_A^-/Q_A which is effective within nano- to milliseconds after the photon absorption event could differ from the equilibrium value due to the electrostatic influence on the Q_A^-/Q_A potential exerted by transiently charged groups (e.g., $P680^+$, Tyr_Z^+, titratable amino acid residues). Also other types of relaxation processes (dielectric relaxation, conformational changes) might affect the working potential. Also, relaxation processes giving rise to sizable entropic contributions to ΔG values might render the second assumption ($\Delta G = e\Delta E_{1/2}$) uncertain. The insufficiently understood relation between possibly time-dependent ΔG values and equilibrium values of redox potentials may represent the most serious uncertainty in the here derived redox-potential estimates.

Earlier estimates of the $P680/P680^+$ potential mostly lead to values of about 1.1 V (see [7] for a critical discussion; for a very early estimate based on delayed fluorescence measurements in the μs-range, see [34]). Recently, a significantly more positive value of +1.26 V has been estimated by an elegant analysis of the recombination decay of the $S_2Q_A^-$ state observed in the second-time range in wildtype and PSII mutants of the cyanobacterium *Synechocystis* [7]. The $P680/P680^+$ potential of [7] is essential identical to the here determined value of +1.25 V. (We note that, in the light of the experimental and conceptual uncertainties, the almost perfect numerical agreement between the potential estimate of the present work and of [7] might be coincidental.)

The estimate of [7] is based on the delayed fluorescence yield of 3% determined for thylakoid preparations of spinach [35]. Since likely there are species-dependent differences in the recombination rate [8], the combination of data obtained for PSII of spinach and *Synechocystis* is not necessarily uncritical. On the other hand, in [36] results have been obtained for *Chlamydomonas reinhardtii*, a unicellular green algae, which are comparable to results previously obtained by the same research group for the cyanobacterium *Synecchocystis* [7] suggesting that there are no relevant difference between the bacterial and green-alga PSII.

In the present study, we refer exclusively to data collected on oxygen-evolving PSII membrane particles. The free-energy differences are calculated from relatively directly determined equilibrium constants and it became possible to estimate the maximal error in the free-energy values. We feel that the thus obtained values for free-energy differences are reasonably precise. The redox-potential values (summarized in Fig. 6) are less certain, but may represent the best estimate we can obtain on basis of the currently available experimental results.

Acknowledgements

We thank Alekos Tsamaloukas for providing the spectra of the prompt and delayed chlorophyll fluorescence, Monika Fünning for the skilled preparation of PSII membrane particles, and Dr. Michael Haumann for stimulating discussions on the subject of the present work. Financial support by the Deutsche Forschungsgemeinschaft (project C6 in the Sfb 498) and the Volkswagenstiftung (electron transfer program) is gratefully acknowledged.

References

[1] A. Zouni, H.-T. Witt, J. Kern, P. Fromme, N. Krauss, W. Saenger, P. Orth, Crystal structure of PSII from *Synechococcus elongatus* ar 3.8 Å resolution, Nature 409 (2001) 739–743.
[2] K.N. Ferreira, T.M. Iverson, K. Maghlaoui, J. Barber, S. Iwata, Architecture of the photosynthetic oxygen-evolving center, Science 303 (2004) 1831–1838.
[3] N. Kamiya, J.-R. Shen, Crystal structure of oxygen-evolving photosystem II from *Thermosynechococcus vulcanus* at 3.7-Å resolution, Proc. Natl. Acad. Sci. U. S. A. 100 (2003) 98–103.
[4] M. Haumann, A. Müller, P. Liebisch, L. Iuzzolino, J. Dittmer, M. Grabolle, T. Neisius, W. Meyer-Klaucke, H. Dau, Structural and oxidation state changes of the photosystem II manganese complex in four transitions of the water oxidation cycle ($S_0 \rightarrow S_1$, $S_1 \rightarrow S_2$, $S_2 \rightarrow S_3$, and $S_{3,4} \rightarrow S_0$) characterized by X-ray absorption spectro-

scopy at 20 K and room temperature, Biochemistry 44 (2005) 1894–1908.
[5] J. Clausen, W. Junge, Detection of an intermediate of photosynthetic water oxidation, Nature 430 (2004) 480–483.
[6] H.J. van Gorkom, Electron transfer in photosystem II, Photosynth. Res. 6 (1985) 97–112.
[7] F. Rappaport, M. Guergova-Kuras, P.J. Nixon, B.A. Diner, J. Lavergne, Kinetics and pathways of charge recombination in photosystem II, Biochemistry 41 (2002) 8518–8527.
[8] R. de Wijn, H.J. van Gorkom, The rate of charge recombination in photosystem II, Biochim. Biophys. Acta 1553 (2002) 302–308.
[9] H. Ishikita, E.-W. Knapp, Redox potentials of chlorophylls and beta-carotene in the antenna complexes of photosystem II, J. Am. Chem. Soc. 127 (2005) 1963–1968.
[10] B.A. Diner, G.T. Babcock, Structure, dynamics, and energy conversion efficiency in photosystem II, in: D.R. Ort, C.F. Yocum (Eds.), Oxygenic Photosynthesis: The Light Reactions, Kluwer Academic Publ, Dordrecht, 1996, pp. 213–247.
[11] H. Dau, K. Sauer, Exciton equilibration and photosystem II exciton dynamics—a fluorescence study on photosystem II membrane particles of spinach, Biochim. Biophys. Acta 1273 (1996) 175–190.
[12] M.J. Schilstra, F. Rappaport, J.H.A. Nugent, C.J. Barnett, D.R. Klug, Proton/hydrogen transfer affects the S-state-dependent microsecond phases of 680+ reduction during water splitting, Biochemistry 37 (1998) 3974–3981.
[13] C. Jeans, M.J. Schilstra, D.R. Klug, The temperature dependence of P680+ reduction in oxygen-evolving photosystem II, Biochemistry 41 (2002) 5015–5023.
[14] E. Schlodder, K. Brettel, H.T. Witt, Relation between microsecond reduction kinetics of photooxidized chlorophyll aII (P-680) and photosynthetic water oxidation, Biochim. Biophys. Acta 808 (1985) 123–131.
[15] G. Renger, Photosynthetic water oxidation to molecular oxygen: apparatus and mechanism, Biochim. Biophys. Acta 1503 (2001) 210–228.
[16] M. Volk, M. Gilbert, G. Rousseau, M. Richter, A. Ogrodnik, M.E. Michel-Beyerle, Similarity of primary radical pair recombination in photosystem II and bacterial reaction centers, FEBS Lett. 336 (1993) 357–362.
[17] H. Schiller, H. Dau, Preparation protocols for high-activity photosystem II membrane particles of green algae and higher plants, pH dependence of oxygen evolution and comparison of the S2-state multiline signal by X-band EPR spectroscopy, J. Photochem. Photobiol., B 55 (2000) 138–144.
[18] A.D. Tsamaloukas, Fluoreszenzspektroskopie zur Excitonendynamik in den Chlorophyll-Antennen des Photosystems II der Pflanzen, Diploma thesis, FB Physik, FU Berlin (2001).
[19] H. Dau, On the relation between absorption and fluorescence emission spectra of photosystems: derivation of a Stepanov relation for pigment clusters, Photosynth. Res. 48 (1996) 139–145.
[20] D. Lazar, Chlorophyll a fluorescence induction, Biochim. Biophys. Acta 1412 (1999) 1–28.
[21] H. Dau, Molecular mechanisms and quantitative models of variable photosystem II fluorescence, Photochem. Photobiol. 1 (1994) 1–23.
[22] P.G. Falkowski, K. Wyman, A.C. Ley, D.C. Mauzerall, Relationship of steady-state photosynthesis to fluorescence in eucaryotic algae, Biochim. Biophys. Acta 849 (1986) 183–193.
[23] A. Melis, P.H. Homann, Kinetic analysis of the fluorescence induction in 3-(3,4-dichlorphenyl)-1,1-dimethylurea poisoned chloroplasts, Photochem. Photobiol. 21 (1975) 431–437.
[24] G.H. Schatz, H. Brock, A.R. Holzwarth, Kinetic and energetic model for the primary processes in photosystem II, Biophys. J. 54 (1988) 397–405.
[25] H.W. Trissl, Long-wavelength absorbing antenna pigments and heterogeneous absorption bands concentrate excitons and increase absorption cross section, Photosynth. Res. 35 (1993) 247–263.
[26] K. Gibasiewicz, A. Dobek, J. Breton, W. Leibl, Modulation of primary radical pair kinetics and energetics in photosystem II by the redox state of the quinone electron acceptor Q(A), Biophys. J. 80 (2001) 1617–1630.
[27] W. Leibl, J. Breton, J. Deprez, H.W. Trissl, Photoelectric study on the kinetics of trapping and charge stabilization in oriented PS II membranes, Photosynth. Res. 22 (1989) 257–275.
[28] A. Krieger, A.W. Rutherford, G.N. Johnson, On the determination of redox midpoint potential of the primary quinone electron acceptor, QA, in Photosystem II, Biochim. Biophys. Acta 1229 (1995) 193–201.
[29] S. Reinman, P. Mathis, Influence of temperature on photosystem II electron transfer reactions, Biochim. Biophys. Acta 635 (1981) 249–258.
[30] P.J. Booth, B. Crystall, I. Ahmad, J. Barber, G. Porter, D.R. Klug, Observation of multiple radical pair states in photosystem II reaction centers, Biochemistry 30 (1991) 7573–7586.
[31] J.M. Hou, V.A. Boichenko, B.A. Diner, D. Mauzerall, Thermodynamics of electron transfer in oxygenic photosynthetic reaction centers: volume change, enthalpy, and entropy of electron-transfer reactions in manganese-depleted photosystem II core complexes, Biochemistry 40 (2001) 7117–7125.
[32] R. Delosme, On some aspects of photosynthesis revealed by photoacoustic studies: a critical evaluation, Photosynth. Res. 76 (2003) 289–301.
[33] R.F. Meiburg, H.J. van Gorkom, R.J. van Dorssen, Excitation trapping and charge separation in photosystem II in the presence of an electrical field, Biochim. Biophys. Acta 724 (1983) 352–358.
[34] P. Jursinic, Govindjee, Temperature dependence of delayed light emission in the 6 to 340 microsecond range after a single flash in chloroplasts, Photochem. Photobiol. 26 (1977) 617–628.
[35] B.G. de Grooth, H.J. van Gorkom, External electric field effects on prompt and delayed fluorescence in chloroplasts, Biochim. Biophys. Acta 635 (1981) 445–456.
[36] A. Cuni, L. Xiong, R. Sayre, F. Rappaport, J. Lavergne, Modification of the pheophytin midpoint potential in photosystem: II. modulation of the quantum yield of charge separation and of charge recombination pathways, Phys. Chem. Chem. Phys. 6 (2004) 4825–4831.